

# SAXS Study of Concentration Fluctuations in the Binary Mixture Hexane-Nitrobenzene

Eric Dufresne, Teamour Nurushev, Roy Clarke, and Steven B. Dierker  
*Department of Physics, University of Michigan, Ann Arbor Michigan 48109-1120*  
(November 8, 1998)

## Abstract

We report the Small Angle X-ray Scattering cross section from composition fluctuations in the binary mixture n-hexane/nitrobenzene near its critical point. Within experimental error, the data analysis of the measured structure factor shows that the intensity and correlation lengths diverge with the expected 3D-Ising critical exponents. We present an approximate relation for predicting scattering rates in an X-ray Photon Correlation Spectroscopy (XPCS) experiment on a binary fluid mixture. We find that the scattering from composition fluctuations in the mixture n-hexane/nitrobenzene, when scaled for a coherent flux of 11.0 keV X-rays equal to  $1.9 \times 10^{10}$  ph/s/ $(5\mu\text{m})^2$ , will yield 10-100 ph/s/speckle for temperatures within 1 °C from the critical temperature and a 1 cm thick sample. Although the correlation times are relatively fast, the scattered intensity per speckle per correlation time will be sufficient to study the critical dynamics of a low molecular weight mixture such as this with XPCS in a range of wavevector inaccessible to visible light PCS.

PACS number(s): 64.60.Fr, 61.10.Eq, 64.70.Ja, 61.25.Em

## I. INTRODUCTION

Due to the large coherent flux of third generation synchrotron sources, the technique of X-ray Photon Correlation Spectroscopy (XPCS) is now performed on an increasing variety of samples [1–7]. In an XPCS experiment, one studies the time correlation function of fluctuations of a speckle pattern [8], which is produced when a beam of coherent X-rays is scattered by spatial inhomogeneities in a material. XPCS has the ability to measure the slow relaxation rate of the dynamic structure factor of materials over a wide range of time scales (1  $\mu$ s-1000 s) in and out of thermodynamic equilibrium at wavevectors inaccessible to visible light (0.004-2  $\text{\AA}^{-1}$ ). The technique of visible PCS [9] allowed for great advances in our understanding of dynamical critical phenomena. XPCS experiments should expand our understanding of short length scale fluctuations, as well as enabling studies of opaque materials like metal alloys.

Most of the results reported to date have been performed on systems with a large length scale microstructure which greatly enhances the scattered intensity due to the coherent addition of the scattering from the large number of atoms in the microstructure. This includes aggregate systems such as colloids [2,3,6] and polymer micelles [5], spinodally decomposing systems such as sodium borosilicate glass [10], and systems with antiphase domains such as metal alloys [1,4,11]. Binary mixtures of small molecular weight fluids have much faster fluctuations ( $\mu$ s to s), and they typically scatter more weakly than systems studied previously. As such, they represent an important test of the general applicability of XPCS to a wide variety of materials.

In this paper we report the scattering rate of composition fluctuations in a binary mixture, n-hexane ( $\text{C}_6\text{H}_{14}$ ) and nitrobenzene ( $\text{C}_6\text{H}_5\text{NO}_2$ ), measured with Small Angle X-ray Scattering (SAXS) on a sample at the critical composition. Although simple binary fluids have been studied extensively by light and neutron scattering techniques [12,13], only one SAXS experiment has been reported *recently* on binary fluids and it did not provide a determination of the absolute scattering intensity from composition fluctuations [14]. It is also interesting to point out that due to the extremely small source size of third generation synchrotron sources and their large increase in brilliance over laboratory sources, our experiment was performed with much better resolution than previous work done on a rotating anode source which was performed with tight collimation in one direction, but no collimation in the other perpendicular direction [14]. This simplifies the data analysis considerably.

The mixture of n-hexane and nitrobenzene has a relatively high X-ray contrast making it a good choice for XPCS. As we show below, when the measured cross section is scaled for a coherent flux of 11.0 keV X-rays equal to  $1.9 \times 10^{10}$  ph/s/ $(5\mu\text{m})^2$ , it should yield a scattering rate of about 10-100 photon/s/speckle for a temperature within 1  $^\circ\text{C}$  from the critical temperature and with a 1 cm thick sample. Our measurements show that it will be feasible to use XPCS to study the dynamics of even such weak scatterers as these low molecular weight hydrocarbon fluid mixtures. This further demonstrates the general applicability of XPCS to a wide variety of materials. Such measurements will also enable tests of the dynamics of critical fluctuations at higher wavevector than previously achievable by visible light PCS.

## II. THEORY AND DATA ANALYSIS

Binary mixtures are in the same universality class as the 3D Ising model [12,14,13]. The structure factor for scattering from concentration fluctuations of a binary mixture can be written as

$$S(q, T) \propto k_B T \chi G(q\xi), \quad (1)$$

where  $G(x)$  is a scaling function,  $T$  the temperature,  $\chi$  the osmotic compressibility,  $q$  the wavevector and  $\xi$  the correlation length of the composition fluctuations [12]. Near the critical point of a continuous phase transition, many physical properties of a system can be expressed as power laws of the reduced temperature  $t = T/T_c - 1$ , where  $T_c$  is the critical temperature.

Previous light scattering measurements on n-hexane/nitrobenzene mixtures determined that the correlation length  $\xi = \xi_0 t^{-\nu}$ , with  $\nu = 0.635 \pm 0.005$  and the bare correlation length  $\xi_0 = 3.54 \pm 0.15$  Å. The osmotic compressibility is found to scale as  $\chi \propto t^{-\gamma}$  with  $\gamma = 1.23 \pm 0.01$  [12]. No exact analytical expression is known for  $G(x)$  for the 3D Ising universality class [12,14,13]. We simply model it with an Ornstein-Zernicke form  $G(x) = (1+x^2)^{-1}$ . Since in our experiment,  $x < 3$ , the Ornstein-Zernicke form is more than adequate to model  $G(x)$  [13]. Thus the measured scattering intensity,  $I(q, T)$ , can be written

$$I(q, T) = \frac{I_0 t^{-\gamma}}{1 + q^2 \xi_0^2 t^{-2\nu}} + B(q), \quad (2)$$

where  $B(q)$  includes parasitic scattering from other materials in the X-ray beam path and a temperature independent structure factor from each of the individual components of the mixture. Izumi [14] has pointed out the importance of measuring this background carefully by measuring the scattering from each individual component in the sample cell and then modeling the background from the individual components as a weighted average of their individual backgrounds.

Since it is difficult to measure  $B(q)$  properly, we chose another approach to model the measured structure factor introduced by Damay et al. [13]. We use the scan performed at the highest temperature  $T_{max}$  as a rough approximation of a background scan and fit the difference

$$I(q, T) - I(q, T_{max}) = I_0 \left[ \frac{t^{-\gamma}}{1 + q^2 \xi_0^2 t^{-2\nu}} - \frac{t_{max}^{-\gamma}}{1 + q^2 \xi_0^2 t_{max}^{-2\nu}} \right], \quad (3)$$

for all the scans with  $T < T_{max}$ . This approach is sufficient when  $B(q)$  is temperature independent and we utilized it in our data analysis. In this fit, the parameters  $I_0$ ,  $T_c$ ,  $\xi_0$ ,  $\nu$ , and  $\gamma$  are optimized by minimizing the  $\chi^2$  of the whole data set. We are able to derive  $B(q)$  by subtracting the small critical scattering contribution from the data at  $T_{max}$ .

## III. EXPERIMENTAL METHOD.

This experiment was performed on the undulator beamline at sector 7 of the Advanced Photon Source, operated by MATT-CAT, the University of Michigan/Howard University/Lucent Technologies-Bell Labs Collaborative Access Team. The fundamental energy of

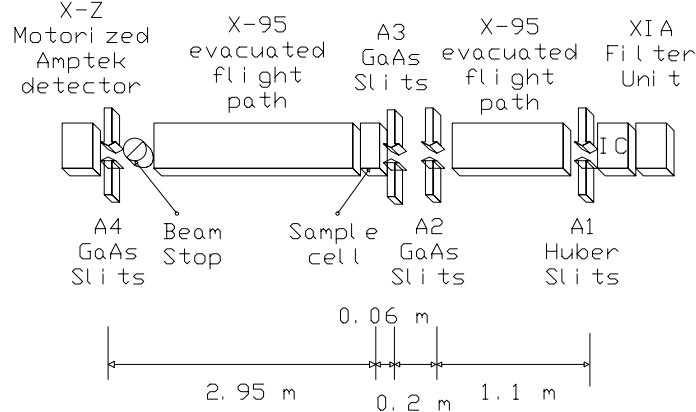


FIG. 1. The experimental set up.

the undulator was set at 11.0 keV. The X-rays generated by the undulator were transmitted through a commissioning window, present for isolation of the vacuum of the storage ring and to absorb the power in the soft X-ray range of the spectrum emitted by the undulator. Four water cooled 254  $\mu\text{m}$  thick Brush-Wellman IF-1 Be windows are also present in the beamline, two of which isolate the monochromator from the rest of the beamline components and the other two are within a few meters of the experimental set up. These windows will be removed in the near future after the commissioning of all the beamline components. Although several Be windows were present in the beamline, the IF-1 grade Be has been found to be one of the the best materials to use for minimizing the parasitic SAXS generated by windows [15].

The full extent of the X-ray beam was incident on our liquid nitrogen cooled double crystal Si (111) monochromator. It was set to diffract 11.0 keV X-rays corresponding to a wavelength  $\lambda_0 = 1.1271 \text{ \AA}$ . The bandpass of the monochromatic spectrum is approximately 0.014 %, which sets a tight longitudinal resolution of  $\Delta k_l = 2\pi/\lambda_0 \times 1.4 \times 10^{-4} = 7.8 \times 10^{-4} \text{ \AA}^{-1}$ .

The experimental set up is schematically shown in Fig. 1. We collimated the monochromatic beam in our experimental hutch with two  $100 \mu\text{m} \times 100 \mu\text{m}$  apertures (A1 and A2 in Fig. 1) defined by slits and separated by approximately 1.1 m. A 1 m long evacuated flight path terminated on each end by a 127  $\mu\text{m}$  IF-1 Be window is placed between the two apertures in order to reduce air absorption and scattering. These two apertures define a characteristic transverse input wavevector acceptance of  $\Delta k = k * 0.1 \text{ mm}/1.1 \text{ m} = 5.1 \times 10^{-4} \text{ \AA}^{-1}$ , where  $k = 2\pi/\lambda_0 = 5.57 \text{ \AA}^{-1}$ . Thus these slits will reject stray parasitic scattering from most of the upstream beamline components in the wavevector range of interest in this experiment (0.003-0.02  $\text{\AA}^{-1}$ ). With a standard air-filled ion chamber, we measured a monochromatic flux of  $7.7 \times 10^{10} \text{ ph/s}/(100\mu\text{m})^2/100\text{mA}$  incident on the sample. In section A, we estimate a flux of  $1.51 \times 10^{11} \text{ ph/s}/(100\mu\text{m})^2/100\text{mA}$  for this beamline configuration, which is within reasonable agreement.

A third guard slit A3 set to  $150 \mu\text{m} \times 150 \mu\text{m}$  and placed approximately 20 cm behind the second slit is used to reduce parasitic scattering from the edges of the second slit. The first aperture was a standard Huber slit. The second and third aperture edges were made by cleaving 0.4 mm thick (100) GaAs wafers. It is well known that GaAs cleaves well in this

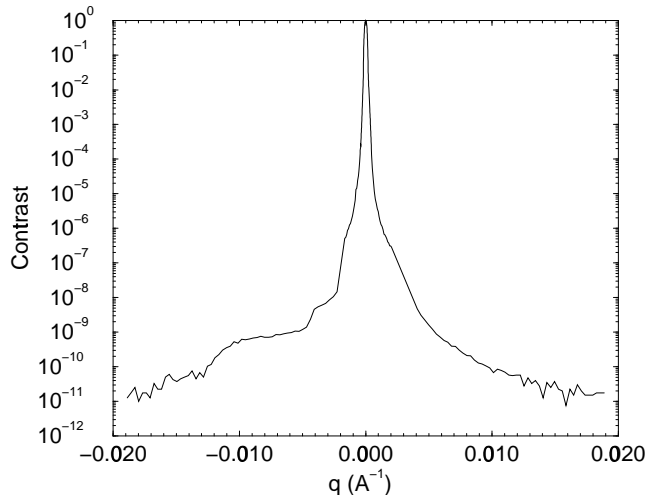


FIG. 2. The experimental SAXS contrast.

direction with atomically flat edges. These edges worked well near 11.0 keV because this energy is above the Ga K edge. The 400  $\mu\text{m}$  thickness corresponds to 23 absorption lengths at 11.0 keV.

Our slit A2 and the source size at the undulator determine the transverse input resolution  $\Delta k_i$ . We approximate the source size by the electron beam rms source size in the horizontal plane  $\sigma_x = 300 \mu\text{m}$  and the vertical plane  $\sigma_y = 60 \mu\text{m}$  [16]. The FWHM angle subtended by the source at a source-sample distance of about 35 m is thus  $\alpha_x = 2.35\sigma_x/35\text{m} \approx 20 \mu\text{rad}$ , while  $\alpha_y \approx 4 \mu\text{rad}$ . The slit opening angle as viewed from the source is  $0.1\text{mm}/35\text{m} = 2.9 \mu\text{rad}$ . For simplicity, adding the two effects in quadrature yields an input resolution  $\Delta k_{ix} = 1.13 \times 10^{-4} \text{ \AA}^{-1}$ , and  $\Delta k_{iy} = 2.75 \times 10^{-5} \text{ \AA}^{-1}$ , well within the angular acceptance of our slits.

The sample was then placed approximately 6 cm from the third slit and a 2.5 m long evacuated flight path was used to reduce air scattering and absorption in front of the detector. At the end of this flight path, a stepper motor driven detector stage could move various detectors in a plane perpendicular to the incoming X-rays. We are able to scan the detector vertically, horizontally or at 45 degrees from the horizontal. This latter direction was most often used because it has the least parasitic scattering from the edges of the horizontal and vertical slit jaws. We measured the parasitic scattering by scanning aperture A4 at  $45^\circ$  from the horizontal in front of the direct beam (see Fig. 2). By opening the detector aperture at larger wavevectors, we can measure over eleven orders of magnitude of signal variation. The small angle parasitic scattering from the optical components was substantially reduced by our set up. Its FWHM was  $2.2 \times 10^{-4} \text{ \AA}^{-1}$ , consistent with the input resolution  $\Delta k_{ix} = 1.13 \times 10^{-4} \text{ \AA}^{-1}$ .

The scattered X-rays were measured with an Amptek XR-100CR detector. This detector has a quantum efficiency  $\epsilon = 0.82$  at 11.0 keV. The detector output was amplified by a fast Canberra 2025 amplifier. The detector resolution was defined by another aperture made with GaAs edges, which was set to  $600 \mu\text{m} \times 600 \mu\text{m}$ , and placed 2.95 m from the sample. It defined a detector resolution  $\Delta q = 600 \mu\text{m} \times 5.57 \text{ \AA}^{-1} / 2.95\text{m} = 1.13 \times 10^{-3} \text{ \AA}^{-1}$ .

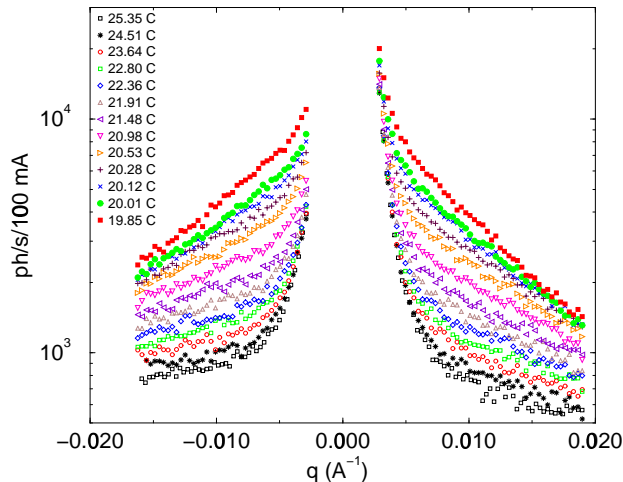


FIG. 3. The measured scattered intensity for the n-hexane/nitrobenzene mixture versus temperature.

The sample was mixed at a critical composition [12] of 41.6 mole % of nitrobenzene by weighing the two components with a precision scale. The critical point was visually checked by finding the temperature where the mixture became milky. The sample cell was a 10 mm thick Al cylinder, sealed by two 2 mil Kapton windows. This cell was mounted on an Al block which was temperature controlled by a closed-loop water bath. The sample temperature, measured with a precision thermistor, was stable to within 20 mK during the duration of a scan. The sample chamber could be moved with a motorized X-Y translation stage. The turbidity of the sample cell could be monitored by lowering the sample cell into the path of a HeNe laser beam and viewing the transmitted light with a video camera. The measured X-ray transmission from the mixture and the two thin Kapton window was 34 %. When the results are normalized for the Kapton window transmission (96.9 %), we find that the sample thickness corresponded to 1.05 X-ray absorption lengths. Using data provided in Table II, the mixture's penetration depth is calculated by weighting each component's mass absorption coefficient  $(\rho\delta)^{-1}$  with its weight fraction, and then multiplying the total mass absorption coefficient by the actual sample density  $\rho_m = 0.852\text{g/cm}^3$ . The calculated sample's X-ray penetration depth is 6.7 mm which compares reasonably well to the measured 9.5 mm deduced from the X-ray measurements.

#### IV. RESULTS

Fig. 3 shows the temperature dependence of the measured SAXS scattering rate for the critical composition. The data has been normalized to a standard beam current of 100 mA. As expected, the scattering rate increases as the temperature is lowered toward  $T_c$ . The left-right asymmetry in the scattering rate is most likely due to an asymmetric background  $B(q)$  (see Fig 4). To fit the data, we used  $T_{max} = 24.51^\circ\text{C}$  and subtracted this scan from all the other data sets. We assumed that the error bars on each scan follow a Poisson distribution. The error bars for the left hand side of Eq. (3) were obtained by adding the

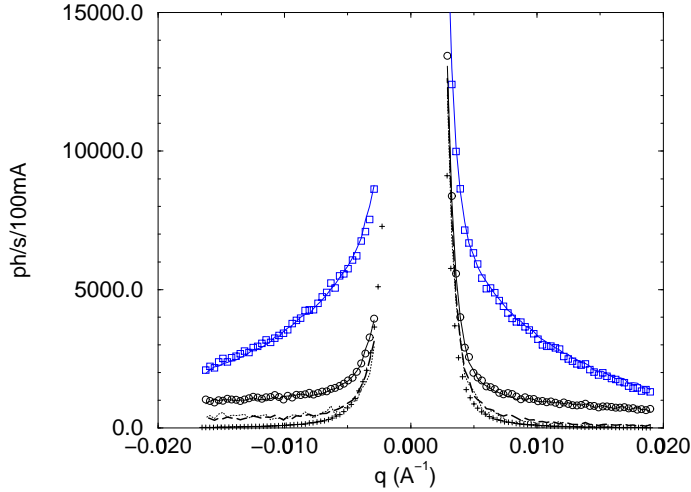


FIG. 4. The measured scattered intensity for two temperatures  $T=20.01$  °C (squares) and  $T=23.64$ °C (circles). The solid lines are fit to Eq. (3). The estimated background for  $T=20.01$  °C (dotted) and  $T=23.64$ °C (dashed) are shown as well as the best estimate of the parasitic scattering from the optics (+).

error bars from each individual scan in quadrature. We fit all the data sets simultaneously to Eq. (3) convolved to the detector resolution  $\Delta q$ .

Fig. 4 shows the results of the fit to all the data for  $20.01 \leq T < 25.35$ °C. The results for the three fit parameters varied were  $T_c = 19.12$  °C,  $\xi_0 = 2.48$  Å, and  $S(q=0) = 4.86$  ph/s/100 mA with a  $\chi^2 = 1.83$ . The measured data and fits for two extreme temperatures are shown,  $T=20.01$  and  $23.64$ °C. The fits are quite good. If one subtracts the critical component of the scattering found in the fit function, one can test for the consistency of the approach. The dashed and dotted line in Fig. 4 represent the maximum variability of the estimated background. The background for negative wavevector is constant over the temperature range but some variations are seen for positive wavevectors. The background is constant far away from  $T_c$ . A better approach would be to use a two pass procedure by first determining the background from the highest temperature scan and then use this background for all the other scans. Fig. 4 also shows our estimate of the background with the sample in the beam. It was obtained by adding the measured background without any sample cell in the beam and the scattering rate from two 2 mil Kapton windows, and then scaling this sum by the measured transmission of the sample. It is clear that the deduced background from the fits are much higher than the estimated parasitic scattering from the beamline and windows, most likely due to molecular scattering from the sample. The deduced background is also asymmetric.

Table I describes in more detail our fitting approach. We performed four types of fits. Type A keeps  $\nu$  and  $\gamma$  fixed, while type A' fits  $\nu$  and  $\gamma$  as well. Type B and B' are similar to A and A' with an additional fitting parameter  $q_0$ , a wavevector offset. The fits are performed on all scans with  $T_{min} \leq T < T_{max}$ . We found that by taking out the scan closest to  $T_c$ ,  $T = 19.85$ °C, the  $\chi^2$  of the fits improved by 30 %. If this scan was included in the analysis, the fits would not converge to reasonable values, and the deduced background for positive

TABLE I. Results of fit parameters to Eq. (3).

$T_{min}$ (°C)	Fit type	$\chi^2$	$q_0$ $\times 10^{-4} \text{Å}^{-1}$	$Sq_0$ ph/s/100mA	$\xi_0$ Å	$T_c$ °C	$\gamma$	$\nu$
19.85	A	2.526	0	$4.23 \pm 0.06$	$2.34 \pm 0.02$	$19.24 \pm 0.01$	1.23	0.635
19.85	B	2.07	$-3.34 \pm 0.23$	$4.26 \pm 0.05$	$2.33 \pm 0.01$	$19.23 \pm 0.01$	1.23	0.635
20.01	A	1.830	0	$4.86 \pm 0.08$	$2.48 \pm 0.02$	$19.12 \pm 0.01$	1.23	0.625
20.01	A'	1.825	0	$6.84 \pm 2.71$	$2.71 \pm 0.40$	$19.19 \pm 0.07$	$1.16 \pm 0.08$	$0.611 \pm 0.034$
20.01	B	1.45	$-3.85 \pm 0.25$	$4.89 \pm 0.07$	$2.46 \pm 0.02$	$19.11 \pm 0.01$	1.23	0.635
20.01	B'	1.446	$-3.84 \pm 0.25$	$6.79 \pm 2.41$	$2.74 \pm 0.36$	$19.16 \pm 0.06$	$1.16 \pm 0.07$	$0.606 \pm 0.031$
20.12	A	1.767	0	$4.81 \pm 0.08$	$2.46 \pm 0.02$	$19.13 \pm 0.02$	1.23	0.635
20.12	A'	1.759	0	$8.92 \pm 4.32$	$3.27 \pm 0.56$	$19.23 \pm 0.09$	$1.10 \pm 0.1$	$0.57 \pm 0.04$
20.12	B	1.375	$-4.67 \pm 0.31$	$4.84 \pm 0.08$	$2.44 \pm 0.02$	$19.11 \pm 0.01$	1.23	0.635
20.12	B'	1.367	$-4.67 \pm 0.31$	$7.01 \pm 3.15$	$3.10 \pm 0.50$	$19.16 \pm 0.09$	$1.16 \pm 0.09$	$0.585 \pm 0.037$
20.28	A	1.684	0	$4.91 \pm 0.10$	$2.49 \pm 0.02$	$19.10 \pm 0.02$	1.23	0.635
20.28	B	1.241	$-6.20 \pm 0.40$	$4.95 \pm 0.09$	$2.46 \pm 0.02$	$19.09 \pm 0.02$	1.23	0.635

wavevector would become negative. When the exponents were kept fixed, the fit converged and the background was positive. With  $T_{min} > 19.85^\circ\text{C}$ , varying the critical exponents becomes possible and the resulting backgrounds are positive. The improvements in  $\chi^2$  from varying the additional two parameters are negligible though, and the resulting critical exponents are typically within error of Ref. [12]. Introducing a wavevector offset improves the  $\chi^2$ , but if we increase  $T_{min}$ , we find that the  $q_0$  increases monotonically. Typically, the fit parameters for type A and B fit are identical within the standard deviations shown, thus there is no need to introduce an offset. All type A fits with  $T_{min} > 19.85^\circ\text{C}$  results in nearly identical fit parameters within error. For future discussion, we will use the results of type A fit for  $T_{min} = 20.01^\circ\text{C}$ .

We can now rescale the fitted model for concentration fluctuations to the absolute volume specific differential cross section given by

$$\frac{d\sigma_V}{d\Omega} = \frac{I(q, T) - B(q)}{\epsilon V I_i e^{-\Delta z/\delta} \Delta\Omega} = \frac{I(q, T) - B(q)}{\epsilon \Delta z F e^{-\Delta z/\delta} \Delta\Omega}, \quad (4)$$

where  $I_i$  is the incident X-ray intensity,  $F = I_i A = 7.7 \times 10^{10}$  ph/s is the total flux in the illuminated area A,  $V = A \Delta z$  is the illuminated volume,  $\Delta z = 1.0$  cm is the sample thickness,  $e^{-\Delta z/\delta} = 0.34$  is the measured sample cell transmission,  $\epsilon = 0.82$  is the quantum efficiency, and  $\Delta\Omega = (600\mu\text{m}/2.95\text{m})^2 = 4.13 \times 10^{-8}$  steradians is the detector solid angle. Using results of the type A fit for  $T_{min} = 20.01^\circ\text{C}$ , the volume specific absolute differential cross section for concentration fluctuation in the mixture n-hexane/nitrobenzene is

$$\frac{d\sigma_V}{d\Omega} = \frac{5.47 \times 10^{-3} \text{cm}^{-1} t^{-\gamma}}{1 + q^2 \xi_0^2 t^{-2\nu}}. \quad (5)$$

## V. DISCUSSION

It is often important to predict the scattering rate from a binary mixture in order to find the materials which have the highest cross section. Following an approach discussed in Ref. [2], one can show that the predicted absolute cross section from a binary mixture is

$$\begin{aligned} \frac{d\sigma_V}{d\Omega} &\approx r_e^2 (\Delta\rho_e)^2 c(1-c) \langle v_0 \rangle t^{-\gamma} G(q\xi) \\ &\approx k^* t^{-\gamma} G(q\xi), \end{aligned} \quad (6)$$

TABLE II. Some physical constant of n-hexane and nitrobenzene.

	n-hexane	nitrobenzene
Chemical formula	C <sub>6</sub> H <sub>6</sub>	C <sub>6</sub> H <sub>5</sub> NO <sub>2</sub>
density (g/cm <sup>3</sup> )	0.659	1.196
molar mass	86.18	123.11
weight fraction in mixture %	49.5	50.5
Z	50	64
volume per molecule (nm <sup>3</sup> )	0.217	0.171
$\rho_e$ (nm <sup>-3</sup> )	230	374.5
$\delta$ (cm)	1.14	0.387

where  $r_e = 2.8 \times 10^{-15}$  m is the classical electron radius,  $(\Delta\rho_e) = 144e/\text{nm}^3$  is the electron density difference between the mixture's components (see Table II),  $c = 0.416$  is the critical composition of nitrobenzene, and  $\langle v_0 \rangle = 0.194 \text{ nm}^3$  is the average molecular volume. The prefactor in Eq. (6) is  $k^* = 7.66 \times 10^{-2} \text{ cm}^{-1}$ , which is a factor 14 more than the measured factor for the cross section in Eq. (5). The difference could be due to the simplifying assumption for the osmotic compressibility in deriving Eq. (6). Note that for strong scattering from a binary system, it is important to have a large electron density difference between the components and a small average electron density for a large X-ray penetration depth. This is the case for hexane/nitrobenzene mixtures.

We next discuss the feasibility of an XPCS experiment on this mixture. If we set a coherent aperture of  $5 \mu\text{m} \times 5 \mu\text{m}$  in front of the sample, we will lose a factor  $(100/5)^2 = 400$  in signal compared to Fig. 3. Similarly in an XPCS experiment with a  $5 \mu\text{m} \times 5 \mu\text{m}$  beam, one must close the slits A4 to limit the detector area to a speckle area. The speckle size is of order  $\lambda R_d/a$ , where  $R_d$  is the sample-detector distance and  $a$  is the aperture size. At 2.95 m, the speckle size is thus  $67 \mu\text{m}$ . This will further reduce the scattering rate by a factor  $(600/67)^2 = 80$ . Fig. 5 shows the predicted coherent scattered intensity per speckle as a function of  $q$  and  $\Delta T$ . We have also assumed a conservative gain of a factor 100 in incident flux due to the use of a “pink beam” produced by a low bandpass X-ray mirror.

The real figure of merit for a PCS experiment is the count rate per speckle per correlation time. For simplicity, we estimate the correlation time with the Stokes-Einstein relation  $\tau = 6\pi\eta\xi/(k_B T q^2)$ , where  $\eta$  is the shear viscosity. The shear viscosity of the n-hexane/nitrobenzene mixture is 0.0053 P [12]. The correlation time can be conveniently written as  $\tau = 4.67 \times 10^{-10} \eta [P] \xi [\text{\AA}] / q^2 [\text{\AA}^{-2}]$ . The correlation time of the fluctuations  $0.1^\circ\text{C}$  away from  $T_c$  for a wavevector of  $0.004 \text{\AA}^{-1}$  is  $61 \mu\text{s}$ , which can be sampled with a standard hardware correlator. In Fig. 5, the product of the calculated correlation time,  $\tau$ , with the predicted count rate per speckle is also shown. Thus with an improvement in X-ray optics by using a “pink beam”, providing an increase in coherent flux of a factor 100 over the current set up, it will be relatively easy to obtain accurate decay rates  $0.1^\circ\text{C}$  away from  $T_c$ .

In summary, we have performed a SAXS study of the binary mixture n-hexane/nitrobenzene near its critical point. We extracted the critical component of the measured scattered intensity from the data by fitting the data to a scaling form. Within the accuracy of the data, the critical exponents observed are consistent with previous light scattering measurements. We reported the absolute X-ray scattering cross section of the

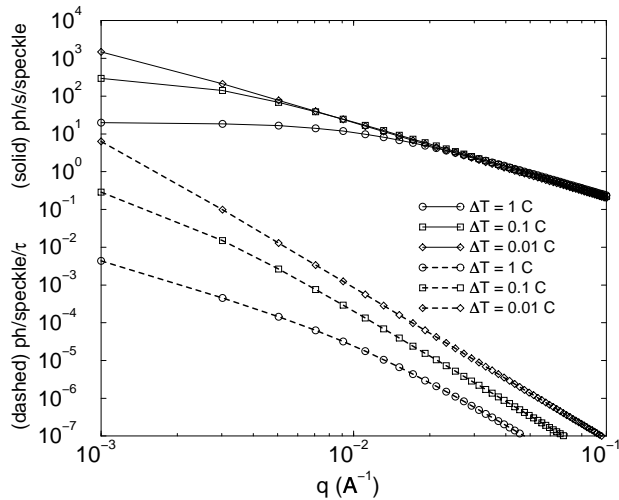


FIG. 5. The predicted scattering rates for n-hexane and nitrobenzene for coherent conditions (solid) for different  $\Delta T = T - T_c$ . The scattering rate per speckle per correlation time (dashed).

mixture and compared it to an approximate theoretical expression. The approach is helpful to determine good candidates for XPCS. This particular mixture is very promising due to its high X-ray contrast and accessible correlation times, which makes it a good candidate for XPCS. We also believe that other fluid mixtures and binary alloys with a conserved order parameter will scatter sufficiently to study critical dynamics in a new range of wavevectors previously inaccessible.

## ACKNOWLEDGMENTS

We are grateful for the support and assistance of Harold Gibson, Try Leng Kruiy, Walter Lowe, Thomas Sanchez and Ernest Williams. We acknowledge support under NSF Grant No. DMR 92-14220, DOE Support through Howard University, and the donors of the Petroleum Research Fund, administered by the American Chemical Society under Grant ACS-PRF No 32105-AC7. Use of the Advanced Photon Source was supported by the U.S. Department of Energy, Basic Energy Sciences, Office of Energy Research, under Contract No. W-31-109-ENG-38.

## APPENDIX A

We simulate the predicted flux for our current optical configuration using the program XOP [17]. The spectrum is generated by the undulator calculation module of XOP, XUS, and then filtered by a commissioning window, four Be windows of 254  $\mu\text{m}$ , a 25  $\mu\text{m}$  thick Al foil and four 127  $\mu\text{m}$  Be windows. The APS parameters measured in Ref. [16] are used for the simulation. The peak spectral flux at 11 keV is  $1.81 \times 10^{12}$  ph/s/0.1%BW after the undulator,  $1.42 \times 10^{12}$  ph/s/0.1%BW after the commissioning window,  $1.29 \times 10^{12}$  ph/s/0.1%BW

after the four beamline Be windows,  $1.14 \times 10^{12}$ ph/s/0.1%BW after the Al foil, and  $1.08 \times 10^{12}$ ph/s/0.1%BW after the four flight path windows. This spectral flux when scaled for the monochromator bandpass  $d\lambda/\lambda = 1.4 \times 10^{-4}$  [18] yields a predicted monochromatic flux of  $1.51 \times 10^{11}$ ph/s/100mA in a  $100 \mu\text{m} \times 100 \mu\text{m}$  aperture, 35 m from the source.

## REFERENCES

- [1] S. Brauer, G. Stephenson, M. Sutton, R. Brüning, E. Dufresne, S. Mochrie, G. Grübel, J. Als-Nielsen, and D. Abernathy, *Phys. Rev. Lett.* **74**, 2010 (1995).
- [2] S. Dierker, R. Pindak, R. Fleming, I. Robinson, and L. Berman, *Phys. Rev. Lett.* **75**, 449 (1995).
- [3] T. Thurn-Albrecht, W. Steffen, A. Patkowski, G. Meier, E. Fischer, G. Grübel, and D. Abernathy, *Phys. Rev. Lett.* **77**, 5437 (1996).
- [4] J. Mainville, F. Bley, F. Livet, E. Geissler, J. Legrand, D. Abernathy, G. Grübel, S. Mochrie, and M. Sutton, *J. Appl. Crystallogr.* **30**, 828 (1997).
- [5] S. Mochrie, A. Mayes, A. Sandy, M. Sutton, S. Brauer, G. Stephenson, D. Abernathy, and G. Grübel, *Phys. Rev. Lett.* **78**, 1275 (1997).
- [6] O. Tsui and S. Mochrie, *Phys. Rev. E* **57**, 2030 (1998).
- [7] A. Poniewierski, R. Holyst, A. Price, L. Sorensen, S. Kevan, and J. Toner, *Phys. Rev. E* **58**, 2027 (1998).
- [8] M. Sutton, S. Mochrie, T. Greytak, S. Nagler, L. Berman, G. Held, and G. Stephenson, *Nature* **352**, 608 (1991).
- [9] B. Chu, *Laser Light Scattering: Basic Principles and Practice*, 2nd ed. (Academic Press, Boston, Toronto, 1991).
- [10] A. Malik, A. Sandy, L. Lurio, G. Stephenson, S. Mochrie, I. McNulty, and M. Sutton, submitted to *Phys. Rev. Lett.* (unpublished).
- [11] E. Dufresne, Ph.D. thesis, McGill University, 1995.
- [12] S.-H. Chen, C.-C. Lai, J. Rouch, and P. Tartaglia, *Phys. Rev. A* **27**, 1086 (1983).
- [13] P. Damay, F. Leclercq, and P. Chieux, *Phys. Rev. B* **40**, 4696 (1989).
- [14] Y. Izumi, *Phys. Rev. A* **39**, 5826 (1989).
- [15] S. Henderson, *J. Appl. Cryst.* **28**, 820 (1995).
- [16] P. Ilinski, R. J. Dejus, E. Gluskin, and T. I. Morrison, in *Optics for High-Brightness Synchrotron Radiation Beamlines II* (SPIE, The International Society for Optical Engineering, P.O. Box 10, Bellingham, Washington 98227-0010 USA, 1996), Vol. 2856, pp. 16-25.
- [17] M. S. del Rio and R. J. Dejus, in *Materials, Manufacturing, and Measurements for Synchrotron Radiation Mirrors* (SPIE, The International Society for Optical Engineering, P.O. Box 10, Bellingham, Washington 98227-0010 USA, 1997), Vol. 3152, pp. 148-157.
- [18] S. Brauer, G. Stephenson, and M. Sutton, *J. Synch. Rad.* **2**, 163 (1995).